Behavior of Built-Up Shear Links Under Large Cyclic Displacement

A.M. ITANI, S. ELFASS, and B.M. DOUGLAS

The towers of the Richmond-San Rafael Bridge (RSRB) play a significant role in the overall bridge seismic behavior and performance. They are responsible for transferring the inertia forces that are generated in the superstructure to the foundation during an earthquake. Therefore, the components of these towers lie in the direct seismic load path and thus any premature failure in these members will interrupt the load path causing inadequate seismic behavior.

The existing towers of the RSRB consisted of chevron braced frames as shown in Figure 1. The chevron braces consist of built-up sections that are connected through double gusset plates. The design for seismic upgrading of these towers was prepared by the California Department of Transportation (Caltrans) by the Gerwick, Severdrup, DMLM Joint Venture (Vincent, 1996). The seismic upgrade consists of removing most of the existing chevron braces and installing dual eccentric braced towers. Thus, the lateral forces are transferred through the new eccentric braced towers while the gravity load is transferred through the existing towers legs. Figure 2 shows the elevation view of the proposed eccentrically braced tower that consists of built-up beams. During severe earthquakes, the links between the eccentric braces become activated and dissipate the input energy by shear yielding. With this controlled yielding, the ultimate capacity and the maximum drift can be quantified to a known level (Vincent, 1996).

Seismic resistant Eccentric Braced Frames (EBF) are lateral load resisting frames that are capable of providing high stiffness in the elastic range and high ductility in the inelastic range. During the 1980s, researchers (Malley and Popov, 1983; Hjelmstad and Popov, 1983; Kasai and Popov, 1986; Engelhardt and Popov, 1989) investigated the cyclic behavior of shear links and established design guidelines that are currently in many seismic provisions. More than sixty shear links with various geometric configurations have been tested by Popov and others under large cyclic displacement (Itani, 1997). A common thread between all these tests is the yielding of the web and the formation of a "ductile fuse." This controlled yielding limits the frame's lateral strength to the ultimate capacity of the shear link.

The viability of EBF in seismic zones is a result of the system's stable plastic rotation while maintaining the lateral strength. Any premature local buckling or fracture in the elements of the shear link would cause an undesirable

A.M. Itani is associate professor of civil engineering, University of Nevada, Reno, NV.

S. Elfass, Bridge Research and Information Center Manager, department of civil engineering, University of Nevada, Reno, NV.

B.M. Douglas, emeritus professor of civil engineering, University of Nevada, Reno, NV.

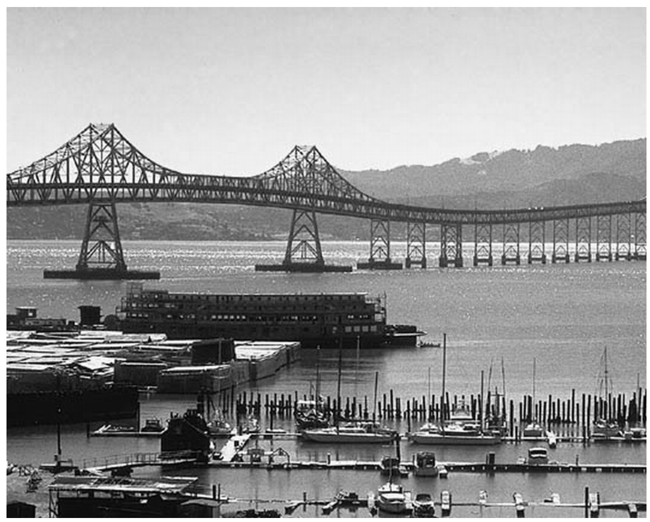

Fig. 1a. View of Richmond San Rafael Bridge.

Fig. 1b. View of Richmond San Rafael towers.

cyclic behavior and response. The design equations that are in the AISC *Seismic Provisions* (AISC, 1997) are tailored towards delaying local and global instabilities of the link until a specified plastic rotation is achieved.

ISSUES RELATED TO BUILT-UP SHEAR LINKS

Figure 2 shows the elevation of the proposed new towers of the RSRB. These towers were designed to achieve a drift capacity of 3 percent of their height (Vincent, 1996). The proportions of the links along the height of the towers have been varied to ensure that they all reach the maximum rotation at approximately the same time. Therefore, built-up links with various proportions were utilized to control the ultimate capacity of the tower. Changing the depth of the link while maintaining the thickness of the web and the dimensions of the flanges, allowed for the capacity control. Structural steel for the flanges and the web for all the links are intended to be taken from the same heat, thus achieving a common predictable yield stress (Vincent, 1996).

Built-up sections have an advantage over rolled shapes because they offer the flexibility of being proportioned to any desired dimensions. Thus, the designer can control the behavior and the ultimate capacity of the section. Furthermore, steel plates do not have significant variability in the yield stress since their production and rolling processes are simpler than those of the rolled shape sections (Hamburger and Frank, 1994).

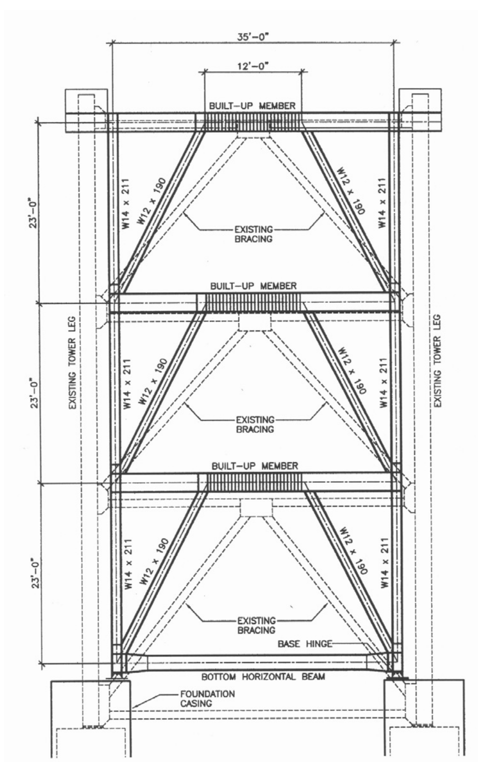

Fig. 2. Elevation of proposed tower retrofit.

OBJECTIVES AND SCOPE

The main objectives of this study were:

1. Investigate the cyclic behavior of built-up shear links designed according to the 1997 AISC *Seismic Provisions.*
2. Collect experimental data on the plastic rotation and ultimate strength of built-up shear links.
3. Assess the performance of the eccentric brace-to-shear link connections.

In order to achieve these objectives two full-scale shear links were tested under cyclic deformations. These links represented the upper and lower bound of the web depth in the proposed retrofit towers of the RSRB.

THE TEST SET-UP

The structural system of the test set-up was chosen to replicate the internal forces of one EBF bay. The sub-assembly was selected to simulate the constraint conditions due to lateral loading on an EBF. Full-scale specimens were used to prevent introduction of scale effect on the response of the links. However, due to limitation of actuator load capacity a one-half EBF bay was used. To have the same internal force effect in a one-half bay as in a full bay, a shear force was applied at the mid-length of the link and a roller support was used at the connection between the beam and the column. Figures 3 to 5 show one-half EBF bay under

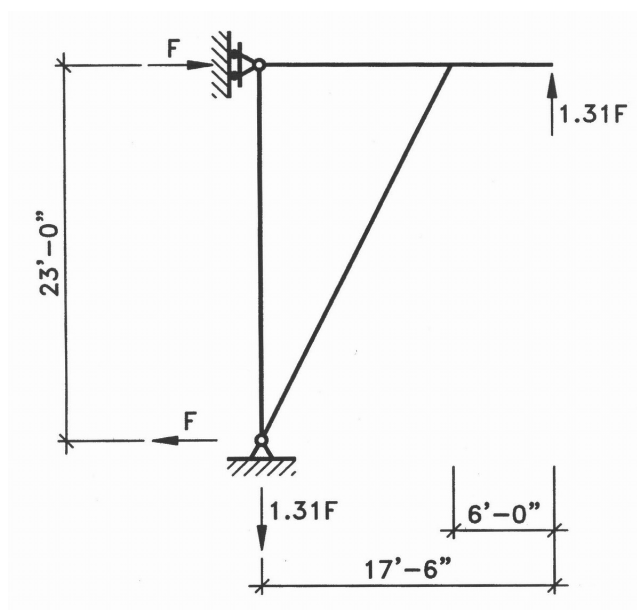

Fig. 3. One-half EBF bay under applied force at link mid length.

applied load at link mid-length and the internal forces due to the applied loading. As can be seen from these figures, the internal forces of the one-half bay are identical to the forces in a full EBF bay.

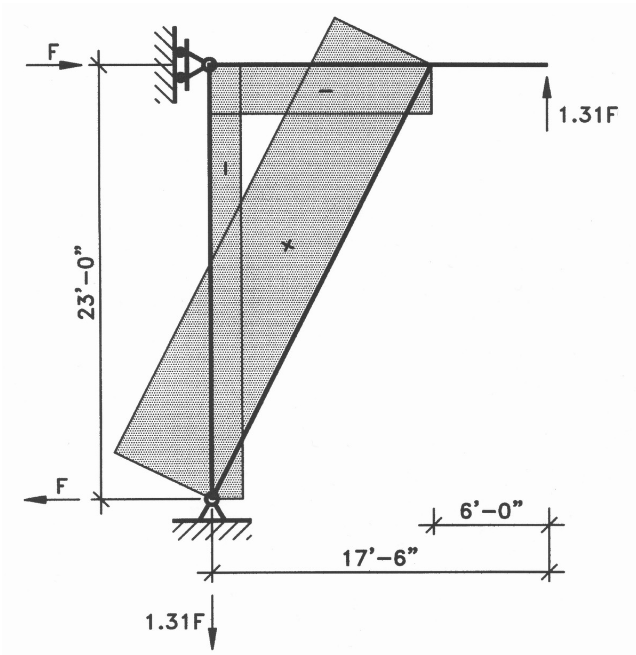

Fig. 4. Normal force diagram under applied force at link mid length.

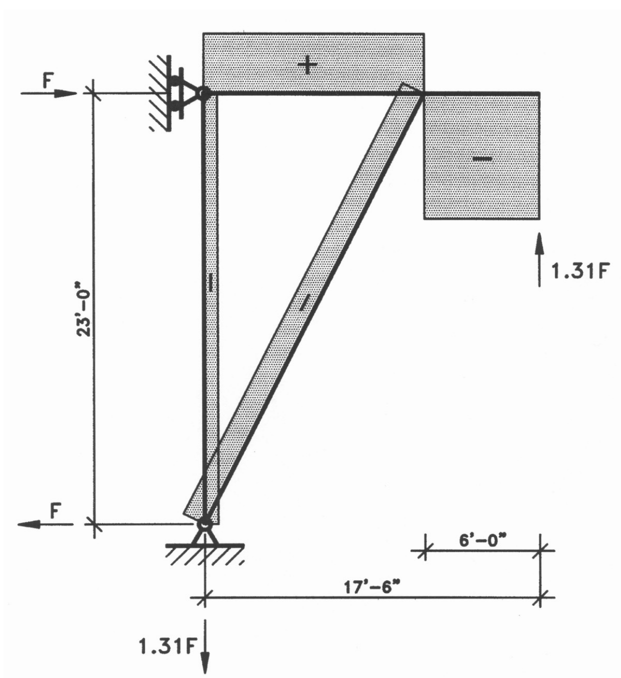

Fig. 5. Shear force diagram under applied force at link mid length.

As indicated in Figure 3, the column is held in place, while the link beam is cycled back and forth. It is apparent that the rigid-plastic kinematics of this subassembly is identical to the one of a full EBF bay.

A schematic representation of the test set-up is shown in Figure 6. The loading unit is composed of double actuators, loading unit, hydraulic pump, and a controller. Two actuators were combined together to apply the cyclic displacement. A loading unit was used to combine the two actuators and apply the load to the link. The push-pull capacity of the two actuators combined is ±750 kips and ±10 in.

TEST SPECIMENS

The links were designed according to the AISC *Seismic Provisions* (AISC, 1997). The length of the link was chosen to be less than $1.6M_p/V_p$. Therefore, the inelastic behavior will be dominated by shear yielding. The flanges and the web of the link complied with the width-thickness ratios that are specified in the seismic provisions. The spacing of the intermediate web stiffeners was based on the AISC specified value of $30t_w–d/5$ to achieve a plastic rotation equal to 0.08 radians.

Two built-up specimens were tested in the experimental program. Specimen 1, BU30, consisted of a built-up section that has a total depth of 30 in. The flanges of BU30 were 14 in. × 1½ in. while the web was 27 in. × ⅜ in. The total length of the beam was equal to 17½ ft and the link portion was equal to 6 ft measured from the pin to the face of the diagonal stiffener as shown in Figure 7.

The flanges were welded to the web using a 5/16-in. fillet weld on the two sides of the web. Two 12⅜ in. × 1 in. continuity plates were added to the built-up section at the intersection with the eccentric brace. These plates were welded to the web and to the top flange using ⅜-in. fillet

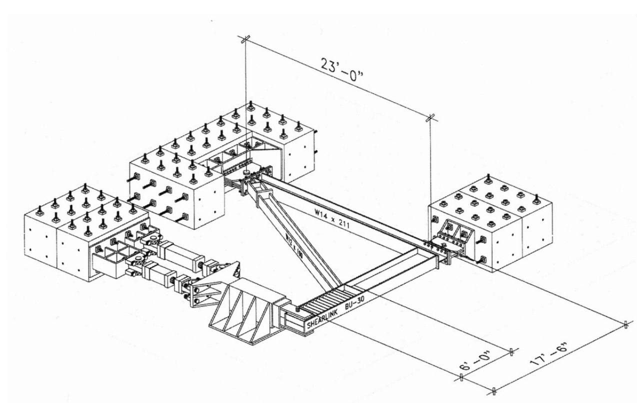

Fig. 6. Schematic view of the test set-up.

welds and a complete-joint-penetration groove (CJP) weld to the bottom flange. A 1-in. thick web doubler plate was added to the panel zone at the intersection with the eccentric brace. Coped holes were used at the four corners of the beam panel zone with a radius equal to 1½ in.

Twelve 6 in. × ⅜ in. stiffeners were mounted on each face of the link. The first stiffener was spaced at 3¾ in. from the continuity plate and the rest were spaced at 5¼ in. based on the equation in the AISC *Seismic Provisions*. Figure 7 shows the details of the test specimen. The intermediate stiffeners were fillet welded to the web and the flanges of the shear link using ¼-in. fillet weld. Three additional stiffeners, 6 in. × ⅜ in., were added outside the link on one face of the web as shown in Figure 7. These additional intermediate stiffeners (outside the shear link) were designed and spaced according to the AASHTO *Standard Specifications* (AASHTO, 1996) to prevent any web buckling due to the presence of the axial force and large bending moment in that region.

The eccentric brace, W12×190, was welded to the bottom flange using complete-joint-penetration groove welds. The welding sequence was specified on the structural drawings as:

> *The CJP groove weld of the continuity plates to the bottom flange and the CJP weld of the web infill plate to the bottom flange shall be complete prior to welding the web and web infill plate to the continuity plate. The fillet weld attaching the continuity plates and the web infill plate to the underside of the top flange shall be the last weld made.*

The bottom end of the eccentric brace was bolted to a stub member as shown in Figure 6 in order to remove and replace the test specimens.

The second specimen, BU16, consisted of a built-up beam with a total depth of 16 in. Figure 8 shows the dimensions and details of BU16.

Lateral support was provided at the top and bottom flanges at the end of the link next to the eccentric brace connection. A W10×68 section was used at the top and bottom flange of the link as a lateral support as shown in Figure 9.

MATERIAL PROPERTIES

Caltrans Standard Specifications (Caltrans, 92) and RSRB Special Provisions were used to specify materials and the fabrication process. The material section in the RSRB Special Provisions stated:

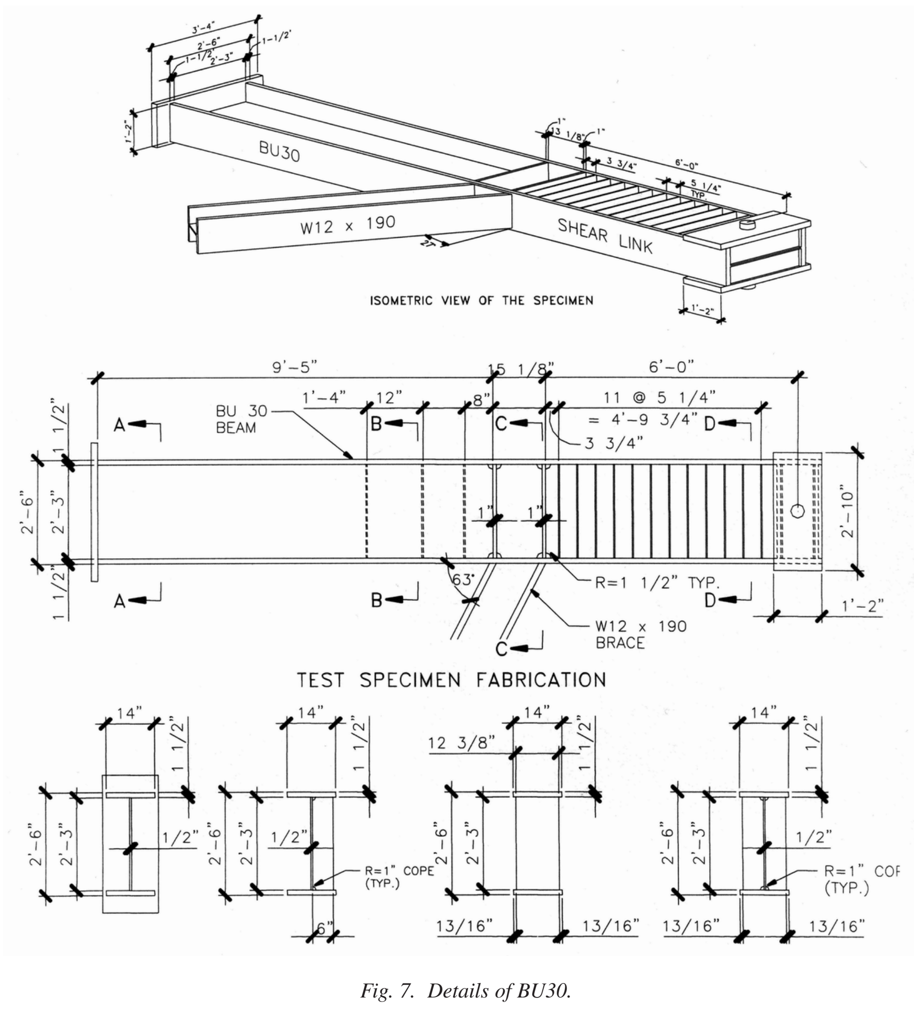

Fig. 7. Details of BU30.

Table 1. Mechanical Properties of Web Material Using ASTM A6 8-in.-Gauge Coupons

Coupon	F_{ya} (ksi)	F_u (ksi)	Fracture Strain (in./in.)
L1	59	82	19
L2	60	82	20
P1	54	80	21
P2	54	78	20
I1	58	80	14
I2	59	81	11

The material for the link beam member flanges and web shall conform to ASTM Designation: A709/A709M Grade 50T2. Ultrasonic testing shall conform to the provisions of ASTM Designation: A578/A578M. Material shall conform to acceptance standard level III. In addition, the maximum yield strength for the material used for the link beam member flanges and webs shall have maximum yield strength no greater than 60 ksi.

Six 18-in. long ASTM A6 coupons with gauge length of 8 in. × ³⁄₈ in. were tested using Instron 4210 with hydraulic grips and laser extensometer. To trace the stress-strain curve of the web, coupons were removed from the following web locations:

- Parallel to direction of rolling, specimens L1 and L2
- Inclination of 45° to direction of rolling, specimens I1 and I2
- Perpendicular to direction of rolling, specimens P1 and P2

The L specimens were oriented along the longitudinal direction of the shear link. The average yield stress and ultimate strength of coupons L1, L2, P1, and P2 is equal to 57 ksi and 81 ksi, respectively. It is interesting to note here that L1 and L2 coupons have the highest yield stress, while P1 and P2 coupons have the lowest yield stress. Also, the fracture strain for L and P coupons was almost identical, while the fracture strain for I coupons was 30 percent less than the fracture strain of L and P coupons. Table 1 lists the test results of these coupons. The average yield stress and

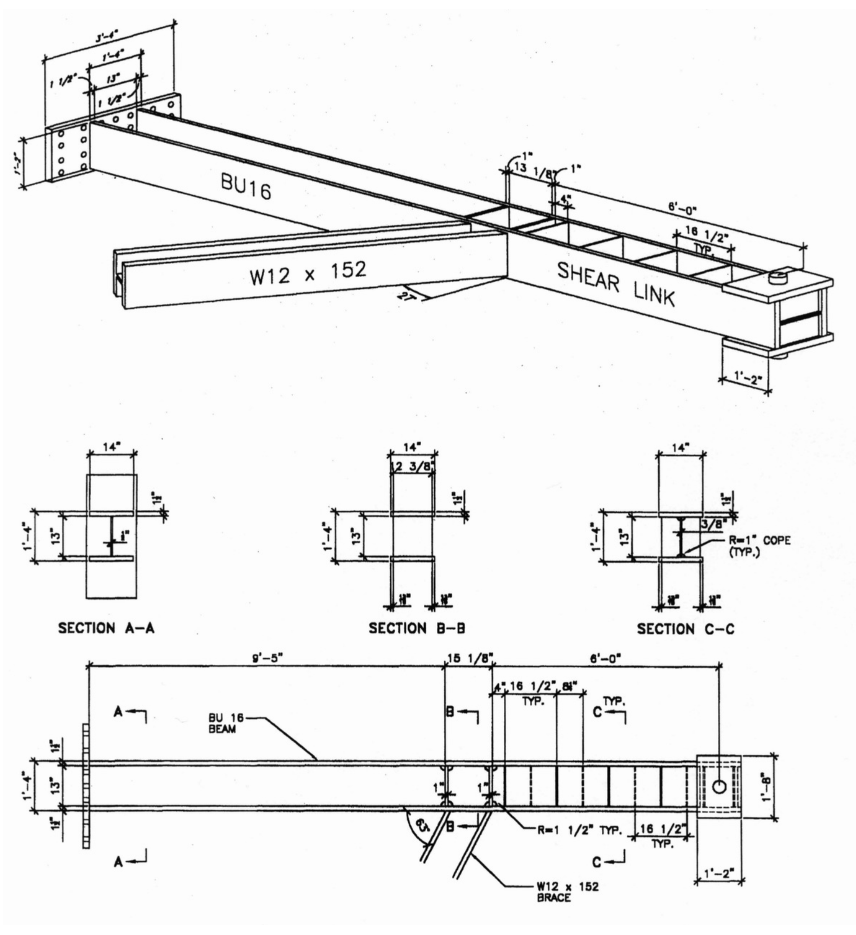

Fig. 8. Details of BU16.

ultimate strength of the flanges of the shear link were equal to 54 ksi and 84 ksi, respectively.

TEST SPECIMEN FABRICATION

Christie Constructors, Inc., Richmond, CA fabricated the test specimens. The fabrication was performed according to Caltrans Standard Specifications and AASHTO/AWS D1.5 Provisions. The fabricator developed the Welding Procedure Specifications (WPS) that were reviewed and approved by Caltrans representatives. A Certified Welding Inspector (CWI), as per the AWS-QC-1 standards, from Testing Engineers, Inc., Oakland, CA inspected and approved the fabrication of the test specimens according to AWS D1.5 requirements.

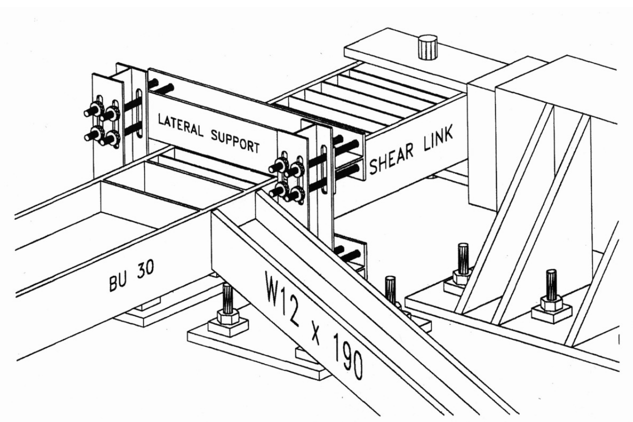

Fig. 9. Schematic view of the lateral support.

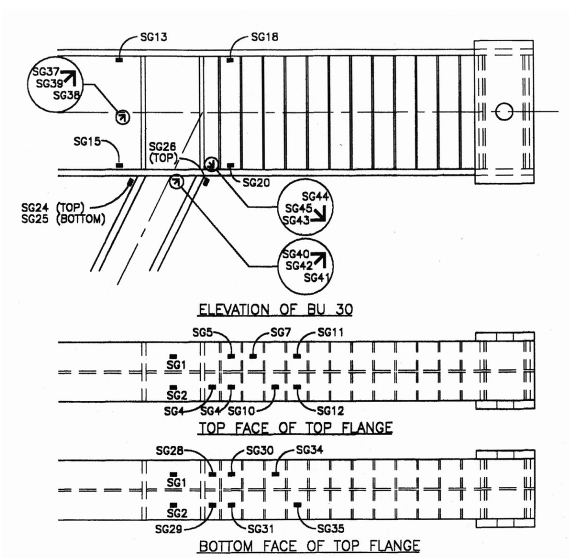

Fig. 10. Location of strain gauge and rosettas in BU 30.

Gas metal arc welding (GMAW) was used to weld the test specimens. The electrodes for GMAW conformed to the requirements of AWS A5.18 Specification for Carbon Steel Filler Metals for Gas Shielded Arc Welding with classification ER 70S-2. All welders that worked on the test specimens were qualified by the tests described in AWS D1.5 and their qualifications were verified by the CWI. The welding parameters including volts, amps, wire feed speed, and arc travel speed, were within the recommended ranges set by electrode manufacturer from the approved AWS specifications and classifications.

The minimum pre-heat and inter-pass temperatures for members up to ¾ in. is 50 °F, over ¾ in. thru 1½ in. is 100 °F, and over 1½ in. through 2½ in. is 200 °F. All weld passes were made using stringer beads with no weaving or wash passes. Except for the root pass, passes did not connect the sides of the weld groove. Also, except for the root and the final passes, peening was performed to each pass when the weld is at a temperature of 150-500 °F. Peening was performed with a slag gun at right angles to the weld making five to six passes along the length of the weld and using a dull tool to prevent sharp notches and cuts. Stress relief cope holes in the webs were used to allow the weld joint and back-up plates to be continuous. Stress relief copes were ground to remove all defects including notches. Back-plates and run-off plates were removed and cleaned according to the AWS D1.5 Specifications.

INSTRUMENTATION

Strain gauges and rosettes were mounted on various locations of each test specimen as shown in Figure 10. Cable extension transducers were used to measure the displacement profile along the beam as shown in Figure 11. All these devices were connected to a data acquisition system with a sampling rate of two readings per second.

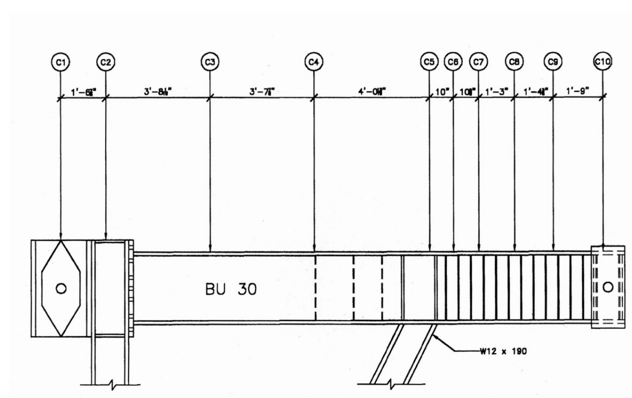

Fig. 11. Location of wire potentiometer.

Table 2. Geometric Ratios of Previously Tested Links and the Built-Up Specimens

Ratio	Previous Test Ranges (Kasai and Popov, 1986)	BU30	BU16
t_f/t_w	1.2-1.67	4	4
$b/2t_f$	5.4-9.6	4.67	4.67
D/t_w	40-57	72	34.7
a/t_w	21-57	14	21.3
a/D	0.42-2.4	0.19	0.62

Table 3. Shear Capacity of Test Specimens Using Nominal Yield Stress

Specimen	M_p (k-ft)	V_p (kips)	e (ft)	$1.6M_p/V_p$ (ft)	$2M_p/e$ (kips)	V_n (kips)
BU30	2,779	304	12	15.3	463	304
BU16	1,335	146	12	16.7	223	146

Table 4. Nominal, Expected and Actual Shear Capacity of Test Specimens

Specimen	V_p	V_{pe}	V_{pa}	R_y	R_{ya}
BU30	304	334	353	1.1	1.16
BU16	146	161	170	1.1	1.16

CAPACITY OF TEST SPECIMENS

Some of the proportions of the two built-up shear links fell outside the ranges of previously tested shear links. Kasai and Popov (1986) collected data of thirty shear links that were tested by Popov and others. Table 2 shows a comparison between the proportions of the shear links that were reported by Kasai and the two test specimens. As can be seen from this table, the built-up shear links are significantly different from the previously tested shear links specifically in the values of t_f/t_w, D/t_w, a/t_w and a/D.

FLEXURAL AND SHEAR STRENGTH

The satisfactory cyclic performance of shear links depends mainly on the ratio between shear and flexural capacity. The yield mechanism for the link can be identified as follows:

- Development of plastic hinges at the ends of the link.
- Development of plastic hinges at the ends of the link in the presence of high shear.
- Development of shear yielding accompanied with yielding at the ends of the link.

The expected plastic moment capacity of the section is equal to

$M_{pe} = Z\,F_{ye}$

where

F_{ye} = the expected yield stress based on the AISC *Seismic Provisions* (AISC, 1997)

$F_{ye} = R_y\,F_y$

The value of R_y for steel plate is equal to 1.1 for A572 Grade 50 steel.

The plastic shear capacity is equal to:

$$V_p = 0.6\,F_y\,(d - 2t_f)\,t_w$$

According to the AISC *Seismic Provisions*, the nominal shear strength of the link is equal to the lesser of V_p or $2\,M_p/e$, where e is the link length. Table 3 presents the nominal shear of the two test specimens, BU30 and BU16. Based on this table it is clear that the test specimens will be dominated by web yielding since e is less than $1.6M_p/V_p$.

Table 4 shows the difference between the expected yield shear strength (V_{pe}) and the actual shear strength (V_{pa}). As can be seen from this table, the value of R_y recommended by AISC for A572 Grade 50 steel underestimates the actual capacity by almost 6 percent.

PLASTIC ROTATION

According to AISC *Seismic Provisions* (AISC, 1997), the plastic rotation for links of lengths 1.6 M_p/V_p or less with intermediate web stiffeners spaced at intervals not exceeding ($30t_w - d/5$) should be at least 0.08 radians. The plastic rotation is defined as the inelastic angle between the link and the beam outside of the link. For BU30 and BU16 the value of 1.6 M_p/V_p is equal 15.3 ft and 16.7 ft, respectively, which exceed the specified 12 ft link length. In addition, the web stiffener spacing for the two shear links satisfied the specified spacing in the AISC requirements.

LOADING HISTORY

The loading history was specified according to *Guideline for Cyclic Seismic Testing of Components of Steel Structures* (ATC, 1992). The test protocol is shown in Figure 12. The yield displacement, δ_y, was determined experimentally for each BU30 and BU16 specimens.

EXPERIMENTAL TESTING

Specimen BU30

Figure 13 shows the response of specimen BU30. The horizontal axis is the applied displacement while the vertical axis is the shear force resisted by the specimen. The shear force is the combination of the forces measured from the two actuators, while the applied displacement is measured form the wire potentiometer C1. At an applied displacement equal to 1.2 in., the web started to yield. Inclined yield line initiated in most web panels at a load equal to 348 kips. The 1.2 in. displacement was specified as the yield displacement, δ_y, of BU30. The specimen was then subjected to the displacement cycles according to the loading history, caus-

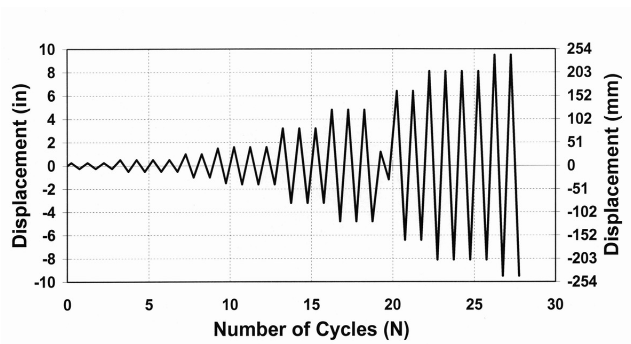

Fig. 12. Loading history.

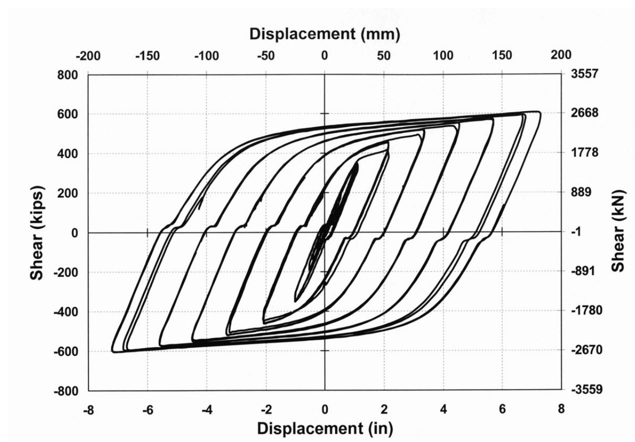

Fig. 13. Force-displacement response of BU30.

Fig. 14. Bottom flange fracture of BU30.

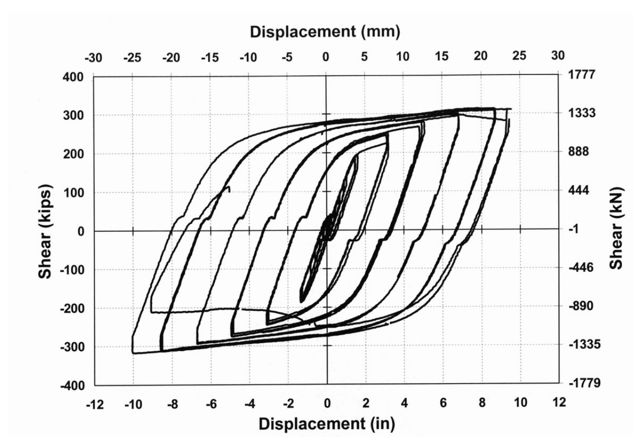

Fig. 15. Force-displacement curve of BU16.

ing web yielding to become more pronounced. As the applied displacement increased to $4\delta_y$ and $5\delta_y$, yielding started to spread outside the web of the link. Yield lines initiated at the top and the bottom flanges of the ends of the shear link. At a displacement of $5\delta_y$ excursion, yielding was observed along the top and bottom link flanges at the edge of the pin plates where the load was applied.

The specimen was then subjected to two cycles at the $6\delta_y$ displacement level with the applied load reaching 600 kips. The web outside the shear link started to yield in addition to more yielding in the top flange. The displacement was then increased to reach 7.68 in., $6.4\delta_y$, representing 8 percent plastic rotation with a corresponding load of 633 kips.

Upon completion of the first cycle at $6.4\delta_y$ and proceeding to the push excursion of the second cycle, a sudden fracture occurred in the bottom flange of the shear link next to the eccentric braced weld. The bottom flange of the shear link was completely fractured as shown in Figure 14. The crack then propagated through the web of the first panel to almost one-third of the web depth. After the fracture, the load dropped to almost zero and the test was stopped.

Specimen BU16

Figure 15 shows the response of specimen BU16 with the vertical and horizontal axes similar to Figure 13. At a displacement equal to 1.5 in., the web started to yield. Yield line initiated in most web panels at a load equal to 185 kips. The 1.5 in. displacement was specified as the yield displacement of BU16. The specimen was subjected to cycles according to the loading history. As the displacement increased to $4\delta_y$ and $5\delta_y$ yielding started to spread along the bottom and top flanges of the link similar to specimen BU30.

The specimen was then subjected to two cycles at $6\delta_y$ displacement level with the applied load reaching 325 kips. Upon completion of the first cycle at $7\delta_y$ and proceeding to the pull excursion of the second cycle, a fracture occurred in the third and fourth web panel as shown in Figure 16. Severe flexural distortion at the flanges of the shear link occurred at the fractured web location. The load capacity deteriorated and reached almost 200 kips. At that level, the test was stopped. After the test, a hairline crack was noticed at the welded connection between the bottom flange and eccentric brace connection.

Fig. 16. Web fracture of BU16.

FRACTURE AND MATERIAL EVALUATION OF BU30 SPECIMEN

The two test specimens showed that the connection between the eccentric brace and the bottom flange of the shear link was susceptible to fracture at high strain levels. Specimen BU30 suffered a complete fracture in the bottom flange while a hairline crack was noticed in Specimen BU16. Schwein/Christensen Laboratory, Lafayette, California, evaluated the connection between BU30 and the eccentric brace. The purpose of this evaluation was to comment on the fracture mode and quality of materials used to fabricate the welded assembly.

Fractographic Examination

The fracture occurred in the lower flange, immediately adjacent to the complete-joint-penetration groove weld joint at the eccentric diagonal intersection. The fracture propagated completely through the bottom flange of the shear link. It arrested after it propagated approximately 6 in. in the web.

The fracture surfaces were examined visually, and with the aid of optical scanning electron microscopes. The fracture features observed indicated a mixed mode of failure. Ductile shear rupture and brittle cleavage zones were both observed in the fracture zone. The fracture features were smeared/crushed along the center-bottom edge of the flange, which may be attributed to compressive load cycling after initial cracking occurred in the bottom flange.

Chevron features on the fracture surface indicate the brittle cleavage zone of fracture initiated near the mid-thickness of the flange directly below the web-cope area. Immediately above and below this point is a zone of ductile shear rupture. It is significant to note that the brittle cleavage fracture did not initiate at a weld defect.

With respect to weld quality, a slight overlap defect was observed at the toe of the weld that connects the web to the link bottom flange at the cope area. Also it appeared that the web cope weld access hole was flame cut without finish grinding. These workmanship flaws do not appear to have presented a significant stress riser to act as an initiation site for brittle fracture.

Link bottom flange thickness measurements indicate a reduction in cross-sectional thickness of up to 7 percent at

Table 5. Mechanical Properties for BU30 Specimen After Cyclic Testing

Sample	BU30 Bottom Flange	BU30 Web	Diagonal Brace Bottom Flange	Required A572 Grade 50
Yield Strength (ksi)[1]	N/A	N/A	58	50
Yield Strength (ksi)[2]	69	97	52	
Tensile Strength (ksi)	86	102	77	65
Elongation in 2 in.	27%	15%	33	21%

[1] Yield strength determined at proportional limit (upper yield point)
[2] Yield strength determined at 0.2% offset method (lower yield point)

Table 6. Charpy V-Notch Toughness Tested at Room Temperature

Sample Location	Absorbed Energy (ft-lb)
Bottom Flange	95.5
	94.3
	108.9
	Average =99.6
Diagonal Brace Bottom Flange	119.2
	95.2
	113.6
	Average=109
Weld Metal	109.6
	107.5
	119.4
	Average =112

the fracture. This reduction in thickness is an indirect indication of some limited plastic deformation in the beam prior to fracture.

Microstructural Examination

A longitudinal cross section was metallurgically prepared from the link flange at the fracture. This included a portion of the heat-affected zone (HAZ) from the CJP weld. A ferritic-pearlitic microstructure was observed in the base metal of the beam flange. This is a normal structure for ASTM A709 Grade 50 steel. The HAZ showed a mixed ferrite-pearlite-banite structure that is commonly observed with non-equilibrium cooling associated with welding.

Mechanical Properties

Base Metal Tensile Tests

Longitudinal tensile coupons were machined from the flanges (at ¼ in. thickness) of the link and the diagonal brace. Both samples were removed from a location within approximately 6 in. of weld fracture area. Additionally, a transverse tensile coupon was machined from the beam web. The samples were tensile tested in accordance with ASTM A370.

The results are shown in Table 5. It is interesting to note here that the sample coupon from the shear link web exhibited a very high yield stress and yield-to-tensile ratio. Additionally, there was no lower yield point observed and the percent elongation was equal to 15 percent. From the results, it can be concluded that the web material was substantially strain hardened as a result of the cyclic testing. Although not as pronounced, a similar trend showing relatively high yield strength was observed in the shear link bottom flange indicating some strain hardening.

Notch Toughness: Base Metal and Weld Metal

Charpy-V-Notch (CVN) impact specimens were machined from the flanges of the beam and diagonal brace. A set of CVN specimens were also machined from the CJP weld near the fracture, that joins the diagonal brace to the bottom flange of the shear link. The CVN specimens were all tested at room temperature (73 °F) in accordance to ASTM

Table 7. Microhardness Test Results of BU30 Connection

Sample Location	Knoop Microhardness	Rockwell Hardness	Approximate Tensile Strength [1] (ksi)
Beam Bottom Flange Base Metal Near Fracture	232	B96	103
	240	B98	109
	243	B98	109
Heat Affected Zone	345	C34	153
	355	C35	157
	338	C33	148

[1] Rockwell hardness and approximate tensile strength values are from published conversion tables.

Table 8. Shear Yield Strength According to Analytical and Experimental Values and Yield Overstrength Ratios

Specimen	Analytical			Experimental	Yield Overstrength	
	V_p	V_{pe}	V_{pa}	V_{pm}	V_{pm}/V_p	V_{pm}/V_{pa}
BU30	304	334	353	348	1.15	0.99
BU16	146	161	170	185	1.27	1.09

A370. The impact test results are shown in Table 6. All three materials (in other words, bottom flange, diagonal brace and CJP weld) exhibited relatively high notch toughness.

Microhardness Test

A Knoop microhardness survey was conducted on the sample previously prepared during the microstructural examination. The hardness was tested in the lower flange base metal and HAZ of the shear link near fracture. The hardness results are shown in Table 7. The average base metal and HAZ hardness was Rockwell B97 and C34, respectively. The base metal hardness is somewhat higher than normal A709 Grade 50 material and is probably due to the work hardening from the cyclic testing. The HAZ hardness indicates some partial banitic phase transformation from non-equilibrium cooling. While the HAZ hardness is on the high side, the levels are below that which is normally associated with hydrogen cracking or embrittlement.

Discussion of Fracture Inspection

The results of the fracture evaluation of a BU30 connection indicated that the materials and workmanship were generally in compliance with the appropriate standards and specifications, with the exception of the slight flaws previously noted at the cope/weld access hole. The extension of the fillet weld into the weld access hole may have contributed to some reduction in plastic rotation by focusing additional stress concentration and localized strain demand in the flange/cope area. The degree to which this flaw diminished the performance is uncertain.

In examining the fracture surface it is evident that there is a significant stress/strain gradient horizontally across and vertically through the shear link bottom flange with the maximum stress concentration just below the web/cope area adjacent to the CJP weld. This stress concentration creates a substantial demand for localized strain/ductility. It is apparent that the connection exhibited some initial ductility as evidenced by the areas on the surface that show ductile shear rupture. Once the demand ductility increased, large tri-axial stresses developed from strain hardening near the web/cope area that resisted further plastic flow, ultimately causing the final brittle cleavage fracture.

ANALYSIS OF EXPERIMENTAL RESULTS LINK YIELD AND ULTIMATE SHEAR STRENGTH

Link Yield Strength

The yield strength of shear links provides an important benchmark during the design process of EBFs. Lateral loading on an EBF, causes a constant shear along the length of the shear link and opposing bending moments at the ends of the link. Therefore, the shear link will be subjected to high shear and high bending moments at its ends. According to perfect plasticity, the presence of the shear and bending moment cause a reduction in both shear strength and flexural strength. This reduction can be predicted analytically using moment-shear (M-V) interaction surfaces. However, experimental data of short shear links conducted by Kasai and Popov (1986) and Engelhardt and Popov (1989) showed that M-V interaction does not exist at the yield limit state. Therefore, the yield strength can be taken as V_p and the flexural strength can be taken as M_p regardless of the magnitude of shear force.

Table 8 presents the values of the shear yield strength based on the specified (V_p), expected (V_{pe}), actual (V_{pa}), and measured (V_{pm}) values for BU30 and BU16. Table 8 also shows the ratios V_{pm} to V_p and V_{pm} to V_{pa}. As can be seen

Table 9. Overstrength Ratios For Shear Ultimate Strength

Specimen	Ω_s	Ω_e	Ω_a	Ω_m
BU30	2.08	1.90	1.79	1.82
BU16	2.12	1.93	1.82	1.68

from this table the specified shear strength underestimated the value by 15 percent and 27 percent for BU30 and BU16, respectively. On the other hand, using the actual value for the web yield stress was able to predict the measured values within 1 percent as Table 8 shows. Therefore, it appears that neglecting the *M-V* interaction and using the actual web yield stress provides a reasonable estimate of the shear yield strength for the tested built-up specimens as in the case of rolled shape short shear links.

Link Ultimate Shear Strength

The basic design philosophy of EBF is to limit the inelastic activity to the link, while all other members, outside the link, stay in the elastic range. Following capacity design procedures, the members outside the link must be designed for the maximum forces generated by the link. Therefore, developing a reasonable overstrength ratio of the link shear force is an important issue in EBF design. Underestimating the maximum shear force that a shear link can generate may lead to a non-ductile behavior such as buckling of the eccentric brace or beam failure outside the link. The commentary of the 1997 AISC *Seismic Provisions* states:

> *The design strength of the diagonal brace is required to exceed the forces corresponding to* R_y *times the nominal shear strength increased 25 percent for strain hardening. That is with* ϕ *equal to 0.85 for axial compression in the brace, the effective overstrength factor (assuming* R_y*=1.1) becomes 1.25(1.1)/0.85 or about, 1.6 for steel with low variability in* F_y *and (assuming* R_y*=1.5) about 2.2 for steel with high variability. With* ϕ *equal to 0.9 for flexure in the beam or diagonal brace, the effective overstrength factor becomes 1,25(1.1)/0.9, or about 1.5, which represent a slight relaxation from the test criterion for steel low variability.*

The commentary also stated that: "*The overstrength factor was developed from tests on typical beams with usual flange thicknesses. For link beam with relatively thick flanges, this factor may need to be increased.*"

Table 8 presents the values of the ultimate shear strength of the test specimens. The overstrength ratio (Ω) for BU30 and BU16 can be determined by dividing the measured ultimate shear strength to yield shear strength. Table 9 shows several over strength ratios based on the measured ultimate shear strength to V_p, V_{pe}, V_{pa}, and V_{pm}. As can be seen from this table, Ω_s was equal to 2.08 and 2.12 for BU30 and BU16, respectively.

As mentioned earlier, link overstrength can be attributed primarily to strain hardening and to the actual yield strength. Using Ω_a as an indicator for the strain hardening ratio, it shows that the two test specimens were subjected to significant strain hardening which can be estimated as 1.79 and 1.82 for BU30 and BU16, respectively.

It is important to note here, that the failure mode of BU30 was the fracture of the shear link bottom flange. Therefore, the force 633 kips at which the bottom flange of the shear link fracture does not represent the actual ultimate shear strength. Based on this investigation, it can be determined that the overstrength factor for BU30 and BU16 is equal to 2.10.

Link End Moment

The magnitude of the link end moment is an important parameter because it dictates the design of the diagonal brace and the beam outside the link. The maximum bending at the end of the shear link ($V_u \times L$) for BU30 and BU16 is equal to 3,798 k-ft and 1,860 k-ft, respectively. These values exceed the M_p for each section by 15 percent and 23 percent for BU30 and BU16, respectively. As discussed previously, the ultimate strength of these built-up links for design purposes has been taken as 2.1 times the yield strength based on simple plastic theory with no *M-V* interaction. This approach would predict the ultimate end moment of 2.1M_p for these links. This indicates that the overstrength 2.1 is high for the flexural design of the beam segment outside the shear link but may be used for the design of the axial forces in the beam segment and the eccentric brace. More experimental tests on built-up shear links will shed more light on this important issue.

Moment-Rotation Relationships at Link Ends

Rotations at the end of the link were determined based on the reading of the wire potentiometers C1 and C6. The rotation, γ, at the end of the shear link is defined by the relative end deflection of the shear link divided by the link length. The rotation is equal to:

$$\gamma = \frac{\delta_1 - \delta_6}{L}$$

where δ_1 and δ_6 is the displacement of wire potentiometer of C1 and C6, and L is the length of the shear link as shown in Figure 17. Figure 18 shows the displacement profile along the beam and the shear link. As shown in the figure, the displacement profile, during the push cycle, between C5 and C2 is almost a straight-line indicating that the shear deformation is dominant. However, the changes in slope between C2 and C1 and C5 and C6 indicate additional bending deformation at these locations as discussed earlier.

A response parameter of greater interest than the total rotation γ is the link plastic rotation angle γ_p. The value γ_p was computed for each specimen as follows (Engelhardt and Popov, 1989):

$$\gamma_p = \gamma - \frac{V_{link}}{k_e}$$

where

V_{link} = shear force in the link

k_e = ratio of V_{link}/γ in the elastic range

For each specimen, k_e was estimated from the measured values of V_{link} and γ in the initial elastic cycles. The value of γ_p computed in this manner includes contributions of inelastic link deformation as well as inelastic link rotation produced by yielding outside the shear link. Figures 19 and 20 show the M-γ_p of the BU30 and BU16. The plastic rotation of the BU30 specimen reached 8 percent radians where the BU16 specimen reached 9.2 percent radians.

CONCLUSIONS

This paper summarized the results of an experimental investigation of two built-up shear links. As expected, the shear dominated the behavior of the two built-up links. The plastic rotational capacity for the two links exceeded the code specified values for such configurations. Based on these tests the following conclusions and observations may be derived:

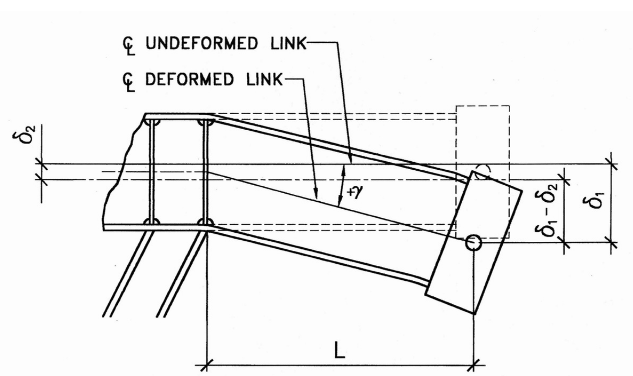

Fig. 17. Rotation link at inflection point.

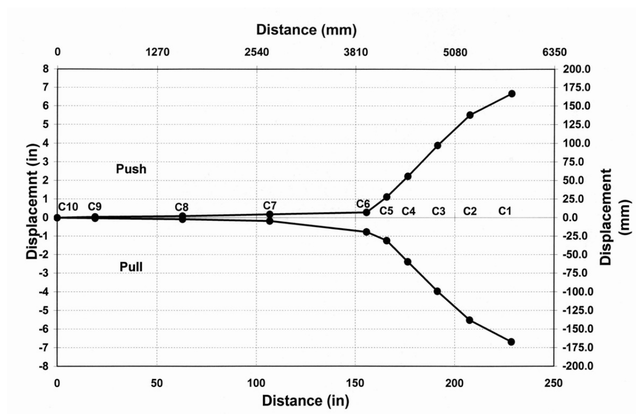

Fig. 18. Deflection profile along BU30 length.

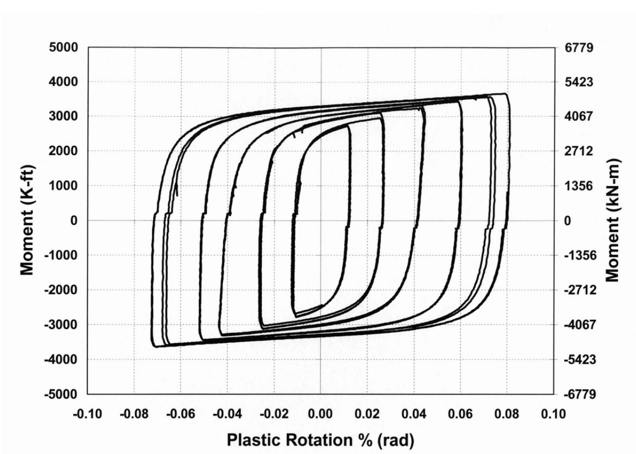

Fig. 19. M-γ_p Response of BU30.

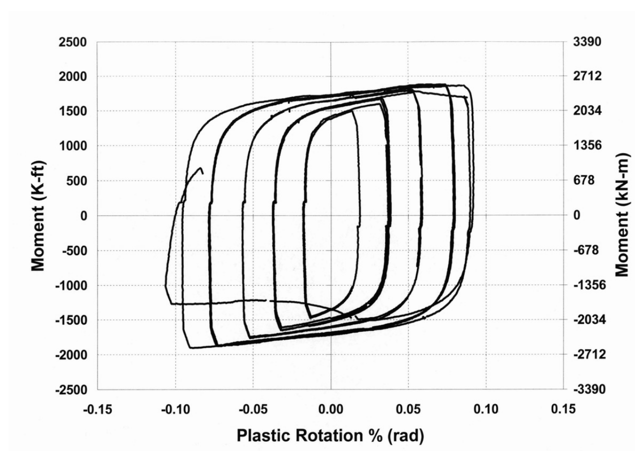

Fig. 20. M-γ_p Response of BU16.

- Built-up shear links designed according to the 1997 AISC Specifications achieved the desired behavior specified in the specification. However, the average overstrength factor for BU30 and BU16 was equal to 2.1, which is almost 31 percent more than the AISC specified value. Therefore, caution should be used in utilizing the AISC overstrength ratio for built-up shear links. Additional experimental investigation is needed to propose an overstrength factor for built-up shear links.

- The brittle facture in the bottom flange of BU30 and hair line crack in weld area of BU16 showed that the eccentric brace connection played an important role in the cyclic behavior of the built-up shear link.

- Both specimens exhibited good ductile behavior and did not show any sign of local buckling in the link web and flanges or lateral-torsional buckling. This indicates that the design equations in the AISC *Seismic Provisions* can be used for the design of built-up shear links.

NOTATIONS

a	=	Stiffener spacing
b	=	Flange width
d	=	Total depth
t_f	=	Flange thickness
t_w	=	Web thickness
F_{ya}	=	Actual yield stress based on coupon testing
F_y	=	Minmum specified yield stress
F_{ye}	=	Expected yield stress
R_y	=	Ratio of expected yield stress F_{ye} to minimum specified yield stress
D	=	Web Depth
M_p	=	Nominal plastic flexural strength
V_p	=	Nominal shear strength of active link
V_{pe}	=	Expected shear strength of active link
V_{pa}	=	Shear strength based on F_{ya}
V_{pm}	=	Measured yield strength on the onset of web yielding
V_u	=	Ultimate web shear capacity measured during experiment
δ_y	=	Measured displacement when yielding initiated in the web panels
Ω_a	=	Ratio of V_u to V_{pa}
Ω_s	=	Ratio of V_u to V_p
Ω_e	=	Ratio of V_u to V_{pe}
Ω_m	=	Ratio of V_u to V_{pm}
δ_1	=	Measured displacement
δ_2	=	Measured displacement
L	=	Distance between center line of the actuator to face of continuity plate
γ	=	Total link rotation
γ_p	=	Plastic link rotation
k_e	=	Ratio of measured shear force to g in the initial elastic cycles

ACKNOWLEDGMENTS

The authors would like to thank the California Department of Transportation for sponsoring the work reported in this paper. Special thanks for Mr. T. Leahy and Mr. A. Akinsanya and other Caltrans engineers for the help and cooperation during this Project. Professor E. Popov comments and advice during the design and the testing phases of the specimens are sincerely appreciated. The cooperation and help from the Gerwick, Severdrup, DMLM Joint Venture is also appreciated. The help of Ms. E. Ware in preparing some of the figures is appreciated.

REFERENCES

American Institute of Steel Construction, Inc. (AISC) (1997), *Seismic Provisions for Structural Steel Buildings*, April 15, Chicago, Illinois.

Malley, J.O. and Popov, E.P. (1983), "Design Considerations for Shear Links in Eccentrically Braced Frames," *Report No. UCB/EERC-83/24*, Earthquake Engineering Research Center, University of California, Berkeley.

Kasai, K. and Popov, E.P. (1986), "A Study of Seismically Resistant Eccentrically Braced Frames," *Report No. UCB/EERC-86/01*, Earthquake Engineering Research Center, University of California, Berkeley.

Engelhardt, M.D. and Popov, E.P. (1989), "Behavior of Long Links in Eccentrically Braced Frames," *Report No. UCB/EERC-89/01*, Earthquake Engineering Research Center, University of California, Berkeley.

Hjelmstad, K.D. and Popov, E.P. (1983), "Seismic Behavior of Active Beam Links in Eccentrically Braced Frames," *Report No. UCB/EERC-83/24*, Earthquake Engineering Research Center, University of California, Berkeley.

California Department of Transportation (Caltrans) (1992), "Standard Specifications," Sacramento, California.

Applied Technology Council (ATC) (1992), *Guidelines for Cyclic Seismic Testing of Components of Steel Structures*, ATC-24, Redwood City, California.

Vincent, J. (1996), "Seismic Retrofit of the Richmond-San Rafael Bridge," 2nd US Seminar on Seismic Design, Evaluation and Retrofit of Steel Bridges, *Report No. UCB/CEE-Steel-96-09*, University of California, Berkeley.

Itani, Ahmad (1997), "Cyclic Behavior of Richmond-San Rafael Tower Links," Report No. CCEER 97-4, Center for Civil Engineering Earthquake Research, University of Nevada, Reno.

American Association of State Highway and Transportation Officials (1996), *Standard Specifications for Highway Bridges*, Washington, D.C.

Hamburger, R. and Frank, K. (1994), "Performance of Welded Steel Moment Connections, Issues Related to Materials and Mechanical Properties," Invitational Workshop on Steel Seismic Issues, SAC Joint Venture, Sept. 8 and 9.